Methodological issues for the mechanical characterization of unfired earth bricks

J.D. Rodríguez-Mariscal, M. Solís*, H. Cifuentes

Escuela Técnica Superior de Ingeniería, Universidad de Sevilla, Camino de los Descubrimientos, 41092 Sevilla, Spain

Abstract

Earth is a traditional building material used through History in many areas around the world. Nowadays, there is also a significant revival of its use because of its ecological value and architectural performance. However, there is still a lack of knowledge about its actual mechanical behavior. This paper is aimed at providing experimental data for the development of consistent methodologies for the characterization of this building material. Compression tests of prismatic, cubic and cylindrical specimens were carried out. The compressive strength, Young modulus and the stress-strain constitutive law are obtained and analyzed. The paper shows that the Unconfined Compression Strength of the material should not be obtained by applying existing correction factors for other materials. The paper also analyzes the meaning and usefulness of different estimates of the Young modulus. Finally, the paper proposes a simplified method for estimating stress-strain relationships from the compressive strength and its corresponding strain of tested samples by using reference normalized curves.

Keywords: earth bricks, compressive behavior, aspect ratio, Young modulus, constitutive law

1. Introduction

Earth is a construction material widely used throughout the world since ancient times. It is estimated that approximately 30% of the world population lives in earth buildings and that in developing countries this percentage rises to approximately 50% [1]. Earth exhibits several attractive features as a building material. It provides good thermal and acoustic isolation properties, it is cheap, easy to handle, and it is a zero polluting and ecological material. The main disadvantage of earth is its poor mechanical properties, which is specially critical in seismic areas [2, 3, 4, 5, 6]. This also limits the use of earth to low-rise buildings, although some exceptions can be found around the world as the well-known city of Shibam (Yemen), where buildings of more than 30m high can be found.

Despite the advantages of the earth as a building material and its extensive use around the world, there is a lack of scientific knowledge about its structural behavior. Hence, there are no rigorous standards for its use, as they exist for other building materials. Only some qualitative and empirical standards currently exist for earthen

*Corresponding author
Email address: msolis@us.es (M. Solís)

construction [7, 8, 9]. The heterogeneity of the constituents of earth and the different building techniques around the world make even more difficult the development of building standards and recommendations. However, there is a need for investigating earth from a mechanical point of view in order to eventually address the needs for building safe and sustainable houses for the large population for which the earth is the only affordable or available building material and also the needs of the rapid developing of earthen modern architecture. Besides, this investigation is required for preserving the valuable existing earthen heritage sites and constructions. Fortunately, there is a increasing interest from the academic research community to address this issue and the numbers of related scientific papers has increased in the last years.

The methodology for the determination of the fundamental mechanical properties such as the compressive strength or the Young modulus of earthen materials is still an open issue. This paper is aimed at providing a new contribution for the development of knowledge about the mechanical behavior of earthen building materials and for the definition of standards for the characterization of its compressive mechanical properties.

There are different traditional techniques for using raw earth as a building material, and different compositions or additives may be used in different areas around the world. Adobe (unfired and air-dried earth blocks use for building adobe masonry constructions) is one of the most widespread technique. This paper is focused on the investigation of the properties of adobe, although it can be useful for future research on other traditional earthen building techniques such as cob or rammed earth, or modern type earthen masonry made of Compressed Earth Blocks (CEB). Although each building technique exhibit its own singularities, there are obviously strong similarities between all of them from a structural point of view.

Values of fundamental mechanical properties of adobe (namely compressive and tensile strength and Young modulus) obtained by different authors have been summarized in [10, 11] and an interesting state of the art review about the tests involved can be found in [12]. The scattering of the experimental results obtained up to now is significant. This is partly due to the different properties of the material (proportions and properties of each constituent, addition of fibers, moisture content, stabilizers, etc) [13, 14, 15, 16], but also due to the different types of tests performed. For instance, the size and shape of the specimens for a standard compressive test is not established. Different sizes of cubic, cylindrical and prismatic specimens can be found in the literature, but the effect of specimen size and shape on the obtained results are not clear yet. Some research works [17, 18, 19, 16] have highlighted the importance of considering the confinement effect on the specimens. They have even illustrated how a low aspect ratio (the ratio between the dimension parallel to the compressive loading direction and the minimum dimension of the cross-section of the specimen) can lead to unreasonable estimations of the compressive strength. In [18, 19] the authors also investigated the application of correction factors (used for other materials) to obtain a consistent value from different types of specimens. This issue have been also addressed for adobe samples of existing constructions [20] and for compressed earth blocks [21].

The Young modulus is probably one of the most uncertain properties of earthen materials [10, 14, 20, 22, 23, 24]. The stress-strain relationship is non-linear and the criteria for the determination of a reference value is not established

yet. Moreover, the experimental procedure to measure strains definitely affects the results [20]. However, some empirical relationships between the compressive strength and the Young modulus have been proposed [7, 8, 24, 20, 10]. The ~~complete~~ stress-strain constitutive law has been also studied by several authors for adobe [20, 25, 12, 23, 26] and also for rammed earth and cob [15, 22]. The complete stress-strain relationship, including not only the rising branch but also the post-peak or softening behavior after the compressive strength is reached, is needed for a complete understanding of the mechanical behavior of the material. This experimental information can be used to asses the compressive fracture energy and develop simplified elastic-plastic models for modelling masonry assemblages [23].

In this research work, simple compression tests are performed on brick, cubic, prismatic and cylindrical specimens. The specimens are made from soils from the riverbank of Guadalquivir river in Sevilla (Spain). To the authors' knowledge, the paper is the first research work about the analysis of mechanical properties from local materials and building techniques in this area. The compressive strength, Young modulus and complete constitutive law are obtained for each type of specimen. Normalized curves are provided and compared to others existing in the literature. The obtained average and normalized stress-strain curves can be useful for future analysis, building numerical models or comparison purposes. In addition, the paper analyzes the influence of the shape of the specimen, the confinement effect, the manufacturing process and the direction of loading (anisotropy) on the experimental results. It also illustrates the need of using a reliable method for the determination of the actual strains and it analyzes several approaches for characterizing the Young modulus.

2. Materials and methods

2.1. Experimental set-up

Specifications from standards for masonry characterization [27] were considered for conducting the tests. Two different loading directions were considered: the vertical (hereafter *longitudinal*) and horizontal (hereafter *transversal*) directions during the molding process (Fig. 1). The *longitudinal* would be equivalent to the usual vertical compressive direction of the bricks as part of an adobe masonry wall, whereas the *transversal* direction would be equivalent to a horizontal compressive one. Thus, considering both directions, information about the anisotropic behavior of the adobe bricks can be obtained.

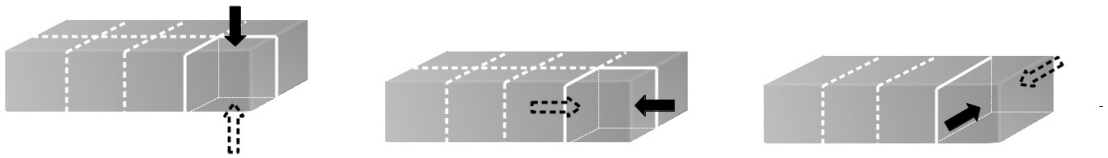

(a) (b) (c)

Figure 1: Scheme of the specimens obtained from cutting the bricks and loading direction: cubes loaded in (a) longitudinal and (b) transversal direction, and (c) prisms

A universal mono-axial servo-hydraulic testing machine was used (50*kN* load capacity and 200*mm* stroke) and all tests were displacement controlled.The applied load and the displacement of the actuator was measured. Two LVDT type displacement sensors (12*mm* range model DC-EC250 from Schaevitz company) measured the relative axial displacement between two points of the prismatic and cylindrical specimens. They were installed at opposite sides of the specimen in order to cancel out any bending effect by computing the average reading of the two sensors. All the output analog signals from the displacement sensors and the testing machine were recorded through a SCXI data acquisition system from National Instruments company.

From the displacement readings, the average strain can be computed. A global strain value for the whole specimen is estimated from the displacement of the actuator, whereas the displacement sensors provide a more local strain value which is not contaminated by the local effects near the contact areas between the specimens and platens of the testing machine. Because of their size, the LVDT displacement sensors could not be used for bricks and cubic specimens. The use of traditional strain gages for obtaining a more precise and local measurement of strains was not feasible because of the dificulty to obtain a proper and effective bond between the gage and the surface of adobe specimen.

The tilt movement of the upper platen of the testing machine was released in order to diminish the effects of irregularities and lack of flatness of the specimen sides, so the load is distributed as uniformly as possible on the specimen. The effect of irregularities is more significant at the first stages of loading [12], as it will be illustrated in next sections.

Table 1 summarizes the description of the different types of specimens and tests performed. The loading direction is indicated as *T* for the *transversal* direction and *L* for the *longitudinal* direction. The type of measuring technique for strain readings is indicated as '*Mach.*' for the displacement of the actuator of the testing machine and *Sen.* for the displacement sensors. The tests were performed complying with the European Standard for the determination of the compressive strength of masonry units [27].

Table 1: Description of the different types of specimens and tests.

Type	Number of tests	Size(mm) width/depth/height	Loading Direction	Loading rate	Strain readings
Bricks	8	320/160/80	L	50kN/min	Mach.
Bricks	6	320/80/160	L	50kN/min	Mach.
Cubes	7	80/80/80	L	3mm/min	Mach.
Cubes	7	80/80/80	T	3mm/min	Mach.
Prisms	22	80/80/160	T	2mm/min	Mach./Sen.
Cylinders	5	150/300	L	4mm/min	Mach. /Sen.

Bricks. ~~A total of 14 adobe bricks were tested: 8 in horizontal position and 6 in vertical position (Fig. 2). The force rate was controlled at 50kN/min, complying with European masonry standards [27].~~

Cubes. Fourteen cubic specimens were tested (Fig. 2), seven of them loaded in the *longitudinal* direction and the other seven were loaded in the *transversal* direction. According to [27], a controlled displacement rate of $3mm/min$ was applied during the tests.

Prisms. Twenty two prismatic specimens were tested (Fig. 2). All of them were tested applying the load parallel to the highest dimension (*transversal* direction). A controlled displacement rate of $2mm/min$ was applied during the tests.

Cylinders. Five cylindrical specimens were tested (Fig. 2). All of them were tested in the vertical direction during the drying process (*longitudinal* direction). A controlled displacement rate of $4mm/min$ was applied during the tests.

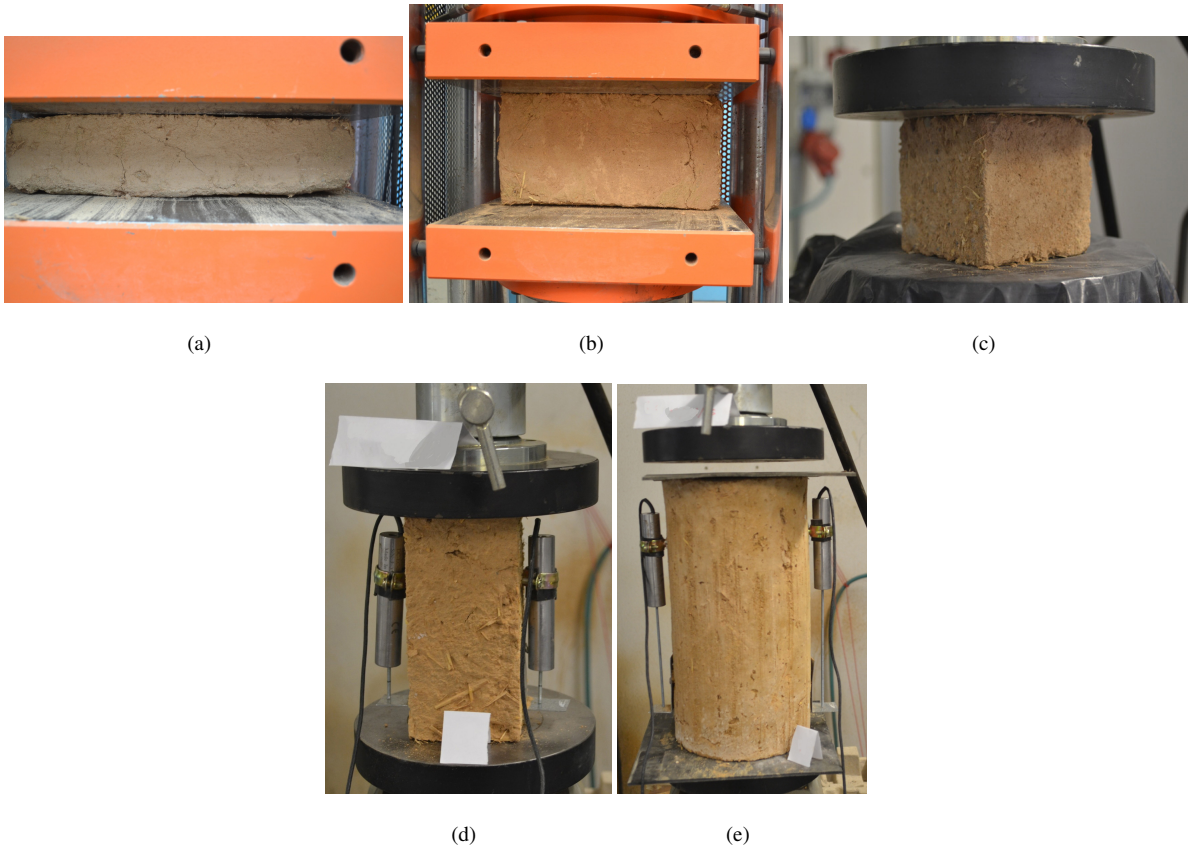

(a) (b) (c)

(d) (e)

Figure 2: Tests of bricks in (a) horizontal and (b) vertical position, (c) cubic, (d) prism and (e) cylindrical specimens.

For each type of specimen, the stress-strain relationships are obtained from the readings of the applied load and the relative displacements (from both the actuator of the testing machine and the displacement sensors). The stress is obtained by simply dividing the load by the area of the cross-section of the specimen. It is assumed that this cross-section remains undeformed, as it is usually considered for other materials like concrete. The strains are obtained by dividing the measured displacement by the original height of the specimen (for the readings from the testing machine)

or the distance between the fixing points of the displacement sensors. The obtained results for the bricks, cubes, prisms and cylinders are presented in next sections. The experimental stress-strain curves for each test are shown and the mean curve of each type of specimen is obtained. This mean curve is approached by a third order polynomial fitting. The polynomial fitting is defined for two different intervals: the first one for strains smaller than the strain corresponding to the peak strength ($\varepsilon_c(\sigma_{c_{max}})$) and the second one for higher strains.

Three stages can be observed during the tests. Initially, there is an adjustment and settlement of the platens on the specimen. This initial stage is influenced by the irregularities and lack of flatness of the sides of the specimen. Strain measurements are not reliable during this stage and the resulting apparent stiffness is very small. This initial stage and its undesirable effect on the stress-strain relationship are more significant when computing strains from the displacement readings of the testing machine. It is also more clearly observed for prismatic and cubic specimens due to their smaller cross-section. During the second stage, a more uniform compression on the whole specimen is achieved, the stiffness increases and the peak strength is reached. Finally, a softening branch on the stress-strain relationship can be observed during the third stage, where large deformations are measured. An asymptotic perfect plastic behavior takes place at about $40-50\%$ of the peak strength.

The next sections include a specific analysis of the stress-strain curves obtained for each type of specimen.

2.2. Experimental results

2.2.1. Experimental stress-strain relationship of bricks.

Adobe masonry is made of bricks of adobe. Therefore, the strength and constitutive law of the adobe material should ideally be obtained from adobe bricks. However, this can not be done in a straightforward way because of the shape of bricks. According to the usual vertical compressive load of any adobe masonry structure, when performing a compressive test on an adobe brick it should be laid horizontally and the load direction should be applied vertically. However, because of the very low slenderness (aspect ratio) of the brick (smaller height than any of the cross-section dimensions), the confinement of the brick between the platens of the testing machine artificially increases the compressive strength. Even when the brick is actually cracked and useless from a structural point of view (Fig. 3), the applied compressive load is still growing. Fig. 4(a) shows the obtained stress-strain relationship for this test. It can be observed that a stress higher than 2.5MPa is reached, and no peak strength is observed. The unrealistic behavior obtained from this type of tests will be illustrated by comparing this result with those shown in next sections for other types of specimens. The confinement phenomenon when testing adobe bricks or rammed earth plates has been also previously reported in the literature [14, 28, 18, 12]. Although the change in the slope of the obtained stress-strain law have been used as an indicator of the compressive strength of the adobe brick [28], this method is unreliable and may provide unrealistic estimations of the actual values. Moreover, because of the handmade manufacturing process of adobe bricks and shrink effects during the drying process, the shape of adobe bricks are usually quite irregular, the external faces may not be parallel to each other and they may be uneven. As a consequence, the scattering of the obtained results may be significantly high. From all these reasons, this type of test

should not be considered for the determination of the compressive behavior of adobe.

Figure 3: Failure mode of a brick tested in horizontal position.

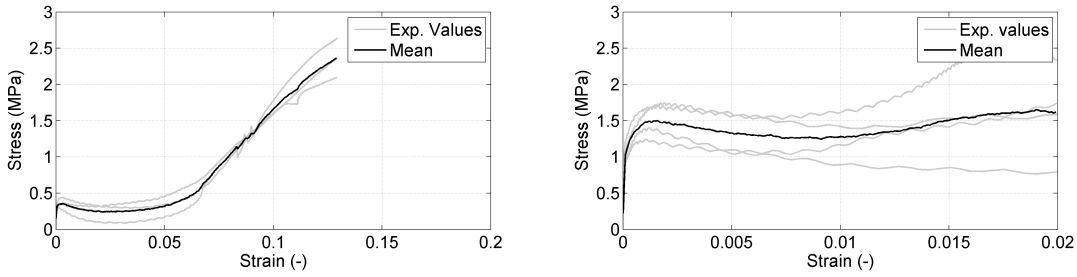

(a) (b)

Figure 4: Stress-strain relationship of bricks tested in (a) horizontal and (b) vertical position.

As a first attempt to circumvent the undesirable confinement effects on adobe bricks, this paper presents the results of compressive tests on adobe bricks laid vertically (the compressive load applied on the largest lateral sides of the brick). The obtained results are shown in Fig. 4(b). Although results are different to those corresponding to the horizontal direction, no reliable nor realistic stress-strain relationship is obtained. Thus, other types of specimens different to adobe bricks should be used. The influence of the specimen size and shape will be discussed in the following sections.

2.2.2. Experimental stress-strain relationship of cubes.

Fig. 5 shows the experimental stress-strain relationships obtained for the cubic specimens when they are loaded in the *longitudinal* (Fig. 5(a)) and *transversal* direction (Fig.5(b)). By comparing both figures, it is clear that there is an anisotropic behavior of the material. The compressive strength and strains are smaller when the load is applied in the *transversal* direction, and the resulting stiffness is higher.

Eqs. (1) and (2) show the third order polynomial curve fitting coefficients for the *longitudinal* and *transversal* directions respectively.

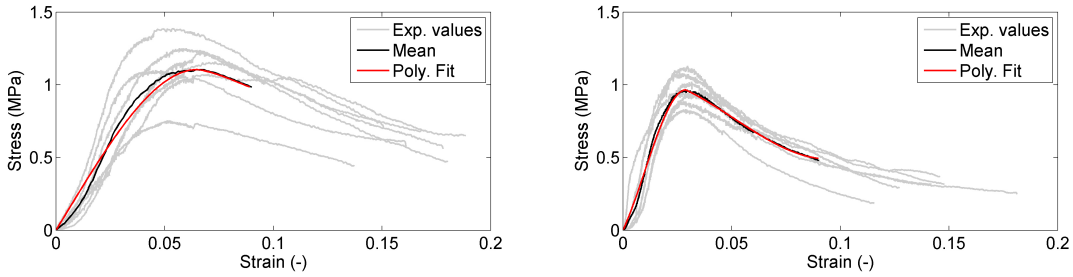

(a) (b)

Figure 5: Stress-strain relationship for cubes loaded in (a) *longitudinal* and (b) *transversal* direction.

$$\sigma_c(\varepsilon_c) = \begin{cases} -2.263e3\varepsilon_c^3 + 32.86\varepsilon_c^2 + 24.41\varepsilon_c & for \quad 0 \leq \varepsilon_c \leq \varepsilon_c(\sigma_c^{max}) \\ 4.657e3\varepsilon_c^3 - 249.50\varepsilon_c^2 - 1.65\varepsilon_c + 1.10 & for \quad \varepsilon_c(\sigma_{c_{max}}) < \varepsilon_c \end{cases} \tag{1}$$

$$\sigma_c(\varepsilon_c) = \begin{cases} -4.137e4\varepsilon_c^3 + 1.236e3\varepsilon_c^2 + 32.20\varepsilon_c & for \quad 0 \leq \varepsilon_c \leq \varepsilon_c(\sigma_{c_{max}}) \\ 1.763e3\varepsilon_c^3 - 116.25\varepsilon_c^2 - 7.18\varepsilon_c + 0.96 & for \quad \varepsilon_c(\sigma_{c_{max}}) < \varepsilon_c \end{cases} \tag{2}$$

2.2.3. Experimental stress-strain relationship of prisms.

Fig. 6 shows the experimental stress-strain relationships for the prismatic specimens. Fig. 6(a) considers the strain measurements obtained from the displacement of the platens of the testing machine, whereas Fig. 6(b) considers the average strain obtained from the relative displacement measured by the two displacement sensors fixed to each specimen. It can be seen from Fig. 6 that the strain measurements from the displacement sensors are smaller than the measurement from the displacement of the platens.

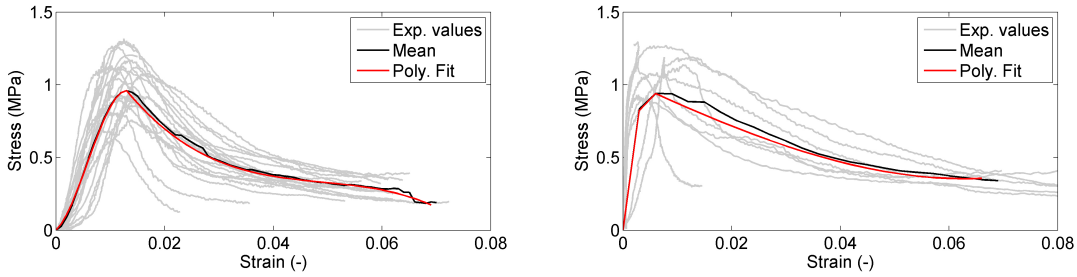

(a) (b)

Figure 6: Stress-strain relationships for prisms obtained from relative displacements measured by (a) the testing machine and (b) the displacement sensors.

Eqs. (3) and (4) show the third order polynomial curve fitting coefficients for the mean curve obtained from the strain measured from the testing machine and from the displacement sensors, respectively.

$$\sigma_c(\varepsilon_c) = \begin{cases} -6.733e5\varepsilon_c^3 + 1.182e4\varepsilon_c^2 + 33.86\varepsilon_c & for \quad 0 \le \varepsilon_c \le \varepsilon_c(\sigma_c^{max}) \\ -1.059e4\varepsilon_c^3 + 1.146e3\varepsilon_c^2 - 45.04\varepsilon_c + 0.959 & for \quad \varepsilon_c(\sigma_{c_{max}}) < \varepsilon_c \end{cases} \tag{3}$$

$$\sigma_c(\varepsilon_c) = \begin{cases} 4.352e6\varepsilon_c^3 - 7.834e4\varepsilon_c^2 + 4.700e2\varepsilon_c & for \quad 0 \le \varepsilon_c \le \varepsilon_c(\sigma_c^{max}) \\ 1.136e3\varepsilon_c^3 + 51.83\varepsilon_c^2 - 16.92\varepsilon_c + 0.94 & for \quad \varepsilon_c(\sigma_{c_{max}}) < \varepsilon_c \end{cases} \tag{4}$$

2.2.4. Experimental stress-strain relationship of cylinders.

Stress-strain curves for cylinders are obtained considering the strains measured from the displacement of the testing machine (Fig. 7(a)) and the displacement sensors (Fig. 7(b)). As for the prisms, the apparent global strain of the specimen computed from the displacement of the platens is overestimated because of the settlement process of the platens on the specimen.

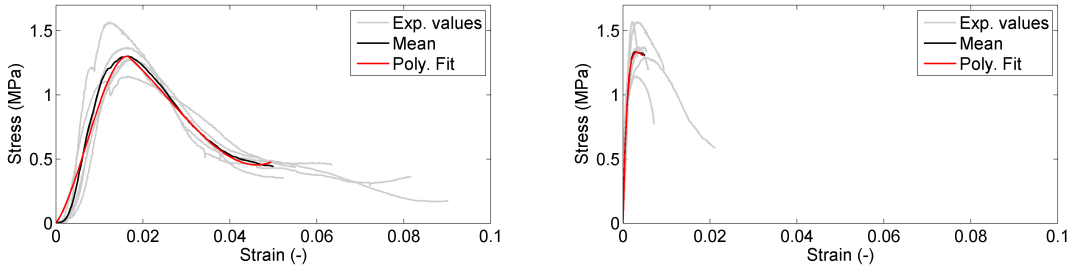

(a) (b)

Figure 7: Stress-strain relationships for cylinders obtained from relative displacements measured by (a) the testing machine and (b) the displacement sensors.

The equations of the polynomial approaches of the mean values of the experimental curves for cylinders are presented for the strains measured from the testing machine (Eq. 5) and from the displacement sensors (Eq.6)

$$\sigma_c(\varepsilon_c) = \begin{cases} -4.026e5\varepsilon_c^3 + 8.502e3\varepsilon_c^2 + 48.22\varepsilon_c & for \quad 0 \le \varepsilon_c \le \varepsilon_c(\sigma_c^{max}) \\ 4.941e4\varepsilon_c^3 - 1.508e3\varepsilon_c^2 - 25.25\varepsilon_c + 1.30 & for \quad \varepsilon_c(\sigma_{c_{max}}) < \varepsilon_c \end{cases} \tag{5}$$

$$\sigma_c(\varepsilon_c) = \begin{cases} 6.030e7\varepsilon_c^3 - 4.940e5\varepsilon_c^2 + 1.385e3\varepsilon_c & for \quad 0 \le \varepsilon_c \le \varepsilon_c(\sigma_c^{max}) \\ -2.214e7\varepsilon_c^3 + 4.3032e4\varepsilon_c^2 - 34.26\varepsilon_c + 1.33 & for \quad \varepsilon_c(\sigma_{c_{max}}) < \varepsilon_c \end{cases} \tag{6}$$

3. Analysis of experimental results

This section analyzes the experimental stress-strain curves obtained from the compression tests shown before. Characteristic values and testing parameters (compressive strength, peak strains, Young modulus, aspect ratio, anisotropy, strain measurement techniques) are determined and analyzed. Moreover, normalized stress-strain relationships are presented and compared with previous results from other authors.

The characteristic values of each magnitude is obtained as the mean value of the obtained experimental set. In addition, the coefficient of variation (CoV) is also provided as an indicator of the scattering of the experimental results. The CoV (%) is defined as the standard deviation divided by the mean value and multiplied by 100.

3.1. Compressive strength, peak strain and anisotropy

The compressive strength is one of the most relevant and basic parameter for the characterization of any building material. However, there is no established methodology for its determination [18]. The knowledge about the influence of the size, shape, capping and manufacturing process on the obtained results is still limited.

The compressive strength for each specimen is obtained as the maximum applied load divided by the area of the cross section of the specimen. The peak strain is defined as the strain corresponding to the compressive strength. Table 2 shows the values obtained for each type of specimen. The direction of the applied load is indicated by (L) and (T) for the *longitudinal* and *transversal* directions respectively.

Table 2: Compressive strength (*MPa*) and peak strain for each type of specimen loaded in the longitudinal (L) or transversal (T) directions.

	$f_{c_k}(CoV\%)$	$\varepsilon_k(CoV\%)$ *machine*	$\varepsilon_k(CoV\%)$ *sensors*
Cubes (T)	0.98 (10.6)	0.029 (14.4)	-
Cubes (L)	1.13 (17.3)	0.060 (17.0)	-
Prisms (T)	1.06 (15.8)	0.013 (27.4)	0.006 (59.6)
Cylinders (L)	1.33 (12.2)	0.016 (12.0)	0.004 (47.5)

It can be seen from Table 2 that the loading direction is affecting the compressive strength, according to the results obtained for the cubes. The difference between the *transversal* and *longitudinal* direction is 13.5% for this type of specimens. Besides, the mode of failure is affected by the loading direction. For loads applied in the *transversal* direction the cracks are parallel to the loading direction (Fig. 8(a)), whereas 45 inclined cracks appear when the load is applied in the *longitudinal* direction (Fig. 8(b)). In addition, the peak strain for the *transversal* direction is approximately one half of the peak strain value for the *longitudinal* direction. This means that stiffness in the *transversal* direction is higher than in the *longitudinal* direction. Thus, the mechanical behavior is significantly different for each loading direction. This anisotropic behavior has been previously reported for extruded rammed earth samples [29, 30, 19], but the authors are not aware of any study on this topic for traditionally manufactured unfired earthen bricks.

This mechanical anisotropy can be explained by the orientation of the clay particles. They can form planar microstructures that can lead to anisotropic properties [30]. During the manufacturing process, the fresh mud is thrown and flattened with the hands during the molding process in order to ensure the mud is filling the mold and to obtain a flat top surface for the brick. As a consequence, the clay platelets are more likely to be horizontally oriented. This leads to a more rigid behavior in the direction parallel to the horizontal clay planes. Because of the same reasons during the

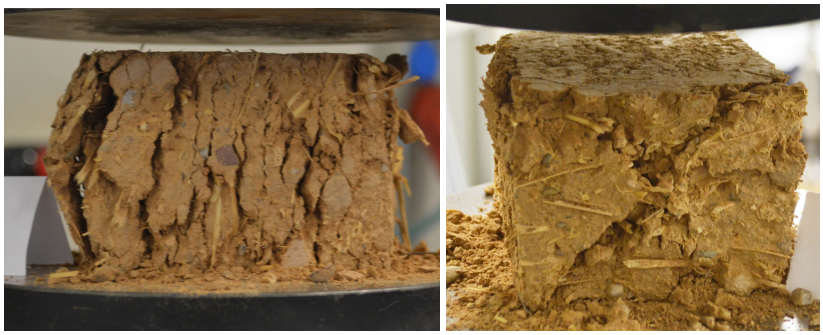

(a) (b)

Figure 8: Typical mode of failure of (a) cubes loaded in *transversal (T)* direction (b) cubes loaded in *longitudinal (L)* direction (c) prisms and (d) cylinders

manufacturing process, there is also a prevailing horizontal orientation of straw fibers. This orientation prevents from cracking by indirect tensile stresses when loaded in the *longitudinal* direction. As a consequence, the compressive strength is higher for this loading direction. On the other hand, the low vertical stiffness of the horizontally oriented straw fibers also contributes to the observed lower rigidity in the *longitudinal* direction. Fig. 9 shows the stress-strain curves for both loading directions and it clearly illustrates the different behavior in terms of stiffness and compressive strength.

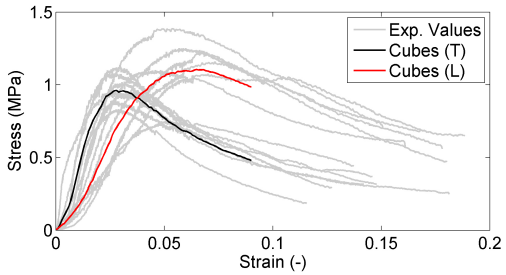

Figure 9: Comparison of stress-strain relationships obtained for cubes loaded in *transversal (T)* and *longitudinal (L)* directions.

The aspect ratio, size, shape and manufacturing process are factors that also affect the results. The cylinders have the same aspect ratio as the prisms, but their shape and size are different. Moreover, the handling of the mud during the manual molding process was different for the cylinders and for the bricks (the cubic and prismatic specimens are pieces of bricks). When filling the cylindrical molds, instead of flattening the mud (which is not feasible because of the size of the cylinder), it is thrown into the mold and compacted with the hands in order to fill possible voids. As a consequence, the cylindrical specimens are somehow made of compressed earth and therefore they can exhibit a higher strength. It must be also noted that the drying process of the cylinders was longer and slower than for the bricks, because it was not possible to remove the mold of the cylinders until they were dry enough (otherwise they would collapse by their self-weight). Therefore, the combination of all these factors make the cylindrical specimens to

behave in a different way than the rest of the specimens, as it will be further illustrated next. This result highlights the importance of using specimens that have been produced following the same procedures and conditions as the bricks.

The influence of the aspect ratio (defined as the height divided by the smallest dimension of the cross section) and the corresponding confinement effect is well known for usual construction materials. The confinement effect is due to the friction between the platens of the testing machine and the specimen that restrains the lateral deformation of the specimen. The influence of the aspect ratio is a key factor in order to develop standards for the determination of the actual compressive strength of the material and to provide consistent values for comparison purposes between different types of samples. The Apparent Compressive Strength (*ACS*) obtained from specimens of specific size and shape can be used to estimate the Unconfined Compressive Strength (UCS) of the material through the use of correction factors. For general masonry units, there are standard correction factors for the estimation of the UCS [27].

However, the influence of the size and shape of the specimen and the confinement effect is not sufficiently studied yet for earthen materials. Previously reported unrealistic compressive strength and peak strain values of earthen materials (higher than $8MPa$ and 20% respectively) [12, 14, 28] show that correction factors are required for earthen materials. Some pioneering efforts have been already made to address this issue [21, 18, 19, 16], but no definite conclusions have been drawn yet.

Table 3 shows the corrected values of the *ACS* for each type of specimen considered in this paper after applying existing correction factors (k_a) suggested for brick masonry [31], soilcrete blocks [32] and masonry units [27] for obtaining the UCS of the material. The corresponding factors for each specimen are obtained by linear interpolation of the values suggested in the aforementioned references for different aspect ratios ($a.r$). Because of the behavior observed for other building materials, these correction factors are higher for higher aspect ratios. Thus, the experimentally obtained *ACS* is expected to be higher for smaller aspect ratios, since the confinement effect becomes more significant. However, the obtained results in this paper exhibit an opposite trend. As a consequence, the application of these existing correction factors do not provide a consistent estimation of the UCS of the material and the uncertainty of the real value of the UCS is more significant. This conflicting trend observed in this paper has been previously reported for cubic specimens of extruded earthen bricks [19]. Table 4 shows the expected ratio of the *ACS* between specimens of aspect ratio 2 ($a.r = 2$) and 1 ($a.r. = 1$) according to each type of correction factors considered and the ratio experimentally obtained in this paper and in [19]. The ratio obtained in [19] ranges from 0.8 to 1.3 for different bricks, but the authors noted that the scattering of the results was significant. In the present paper, similar ratios are obtained for the *longitudinal* (obtained by comparing results from cylinders and cubes) and *transversal* (obtained by comparing prisms and cubes) loading directions (0.85 and 0.92 respectively). In [20] the authors obtained that the ratio between the compressive strength of cubic specimens and cylinders of aspect ratio of 1.8 was 1.06. However, the scattering of the results presented in [20] between different tested bricks was significant and some of them exhibited ratios smaller than unity. Moreover, the confinement effect was reduced by the use of a capping made of a regularization mortar.

A possible explanation for this conflicting phenomenon is the manufacturing process of the earthen specimens. In

Table 3: Estimated values of the Unconfined Compressive Strength (UCS, in MPa) obtained from the experimental Apparent Compressive Strength (ACS, in MPa) from linear interpolation of existing correction factors (k_a) for other materials.

	Tests		Krefeld (1938)		H. and J. (1992)		CNS (2011)	
	ACS	$a.r.$	k_a	UCS	k_a	UCS	k_a	UCS
Cubes (T)	0.98	1	0.7	0.68	0.58	0.56	0.962	0.94
Cubes (L)	1.13	1	0.7	0.79	0.58	0.65	0.962	1.08
Prisms (T)	1.06	2	0.78	0.82	0.74	0.78	1.27	1.34
Cylinders (L)	1.33	2	0.78	1.03	0.74	0.98	1.35	1.79

Table 4: Ratio of the Apparent Compressive Strength (ACS) between specimens of aspect ratio 2 ($a.r = 2$) and 1 ($a.r. = 1$)

	$ACS_{a.r.=1}/ACS_{a.r.=2}$
Krefeld 1938	1.11
Heathcote et al 1992.	1.28
CNS 2011	1.4(L)/1.32(T)
Aubert et al. 2016	0.8-1.3
Silveira et al. 2013	1.06
Present work	0.85(L)/0.92(T)

[19], the authors suggested that the specimens could be damaged when they were obtained by the cutting the bricks. However, in the present research work, no apparent damage was observed by visual inspection on the cubic and prismatic specimens. A more likely reason for this unexpected behavior of earthen specimens is that the influence of the interaction forces between the platens and the faces of the specimen is different to other materials, due to a much lower stiffness and strength. Earthen materials also exhibit different relative ratios between compressive strength, tensile strength and Young modulus that can affect the mode of failure affected by the confinement effect. Nonetheless, it is clear from the previous results presented in [19] and in the present paper that further and more exhaustive research is needed at this point and existing correction factors may lead to erroneous estimations of the UCS of earthen materials. It is worth to notice at this point that Spanish Standard for Compressed Earth Bricks [33] allows the use of correction factors provided in the European Standard for masonry units [27], but the present paper illustrates that this use is not supported by sufficient empirical knowledge on earthen materials.

3.2. Young modulus

The Young modulus is a critical parameter for the characterization of the mechanical behavior of any material. In the case of earthen materials, there is still missing a standard process for its determination. The scattering of the experimental results, the non-linear behavior of the material, the difficulty for measuring strains, etc, make that

additional research work is required to address this issue. Nevertheless, it must be noted that earthen materials are non-linear and inelastic, so a standard determination of the Young modulus can be used just for comparison purposes between different samples and as an indicator of the stiffness of the material, but not to define the stress-strain relationship.

Standards for masonry [27], rocks [34] and other materials [35] consider the almost linear part of the stress-strain curve between 1/3 and 2/3 of the compressive strength for the determination of the Young modulus. According to this, three values of the Young modulus are obtained in this paper: the secant modulus at 1/3 and 2/3 of the compressive strength ($E_{1/3}$ and $E_{2/3}$ respectively) and the tangent modulus (E_m), defined as the slope of the chord drawn between those two points. Table 5 shows the values obtained for each type of specimen along with its corresponding Coefficient of Variation (CoV %).

Table 5: Estimated values (in MPa) of the secant Young modulus at 1/3 ($E_{1/3}$) and 2/3 ($E_{2/3}$) of the compressive strength and the chord modulus (E_m).

	$E_{1/3}(CoV\%)$	$E_{2/3}(CoV\%)$	$E_m(CoV\%)$
Cubes $(T, mach)$	46.88 (71.8)	46.75 (22.7)	60.29 (15.9)
Cubes $(L, mach)$	20.76 (29.4)	25.48 (30.8)	33.21 (33.5)
Prisms $(T, mach)$	77.40 (33.5)	95.03 (31.7)	132.39 (34.8)
Prisms $(T, sens)$	1080.5 (58.51)	721.80 (59.86)	556.73 (58.9)
Cylinders $(L, mach)$	78.03 (28.1)	110.67 (27.1)	195.11 (28.4)
Cylinders $(L, sens)$	1539.2 (51.56)	1005.0 (23.86)	801.96 (23.6)

It is clear from Table 5 that the scattering of the obtained values of the Young modulus is significant. Thus, it is mandatory that when providing any value of Young modulus for an earthen material it must be specified its precise mathematical definition and the experimental method used for measuring strains, otherwise the value is meaningless.

As expected from the previous discussion about the anisotropic behavior encountered for the cubic specimens, higher values of the Young modulus are obtained for the *transversal* direction. For the prisms and cylinders, the values obtained from the strains estimated from the displacement readings of the actuator of the testing machine and from the displacement sensors ($'mach'$ and $'sens'$ in Table 5 respectively) are different (as expected from the stress-strain curves presented in sections 2.2.3 and 2.2.4). The values obtained from the testing machine readings are too small since it implicitly considers as real strains the settlement of the platens on the contact surface, the local crushing on that area and the effect of surface irregularities. Therefore, this method should not be considered as a valid method for measuring strains, for estimating the stress-strain relationship or for estimating any value of the Young modulus. Unfortunately, most of the previously reported values for the Young values of earthen materials have been based on this invalid method and very few data are available for reliable values obtained from displacement sensors (the authors are only aware of the results presented in [20, 26]).

In [20] the strains were measured from displacement sensors but the obtained values of the Young modulus are too

high (from 7 to 25GPa), probably due to the fact that, as the authors said, the tested specimens had a high proportion of lime binder that can significant increase the stiffness of the material. In [26], the authors estimated the chord modulus between 30% and 60% for strains measured from the displacement of the actuator of the testing machine and the secant modulus at $1/3$ of the compressive strength from local strains measured by a Digital Image Correlation system. They obtained a value of 147MPa (CV 27%) and 801MPa (CV 42%) for the first and for the latter estimates of Young modulus, respectively. These values are in agreement with the values obtained in this paper for the prisms for E_m from the displacement sensors (132.39MPa) and for $E_{1/3}$ from the actuator of the testing machine (1080.5MPa), respectively.

Some previously proposed linear correlations between the Young modulus and the compressive strength are far from providing good estimations of a real value of the Young modulus, as they are based on erroneous estimates of global strains from the displacement of the actuator of the testing machine. According to those correlations, the Young modulus can be obtained by multiplying the compressive strength by 300 [8], by 160 [10], by 173 [24] or by 200 [25]. Although these correlations do not specify which type of Young modulus are estimating, they can not provide a realistic estimation according to the values obtained from the displacement sensors in this paper and in [26]. The fact that these correlations are indeed proposed in some earthen building standards illustrates again the fact that additional rigorous and extensive research is needed for the development of reliable Standards.

In this paper, the Young modulus obtained from the displacement sensors readings for prisms and cylinders range approximately between 500 and 1200 times the compressive strength, depending on the type of estimation used for the Young modulus. For both the prisms and the cylinders, it is obtained that $E_{1/3}$ is roughly 50% bigger than $E_{2/3}$ and E_m is roughly 25% smaller than $E_{2/3}$. This paper proposes the use of the chord modulus (E_m) between $1/3$ and $2/3$ of the compressive strength, since it provides a more reasonable estimation of the stiffness of the material when compared to the secant modulus (Fig. 10) and the stress-strain curve exhibits a linear trend in this range.

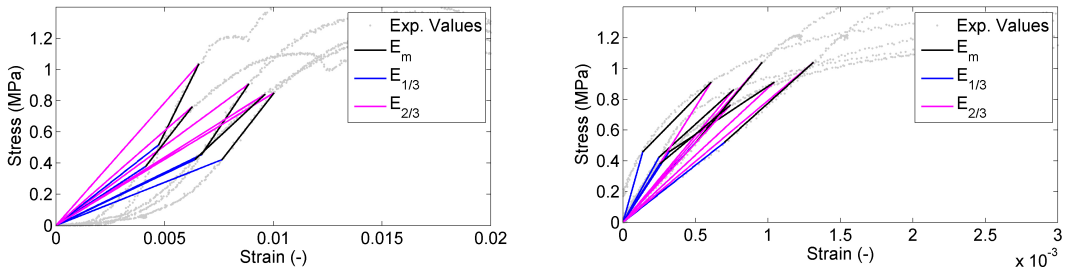

(a) (b)

Figure 10: Comparison of different Young modulus estimates for cylinders. Relative displacements measured by (a) the testing machine and (b) the displacement sensors.

3.3. Normalized stress-strain relationship

In order to compare the stress-strain curves for all types of specimens in a straightforward way, the polynomial curve fitting curves shown in section 2.2 for each type of specimen are normalized so the stresses are divided by their corresponding compressive strength ($\bar{\sigma}_c = \sigma_c / f_{c_k}$) and the strains are divided by their corresponding peak strains ($\bar{\varepsilon}_c = \varepsilon_c / \varepsilon_k$). Thus, all the normalized stress-strain curves go from (0,0) to (1,1). The normalized equations are written in Eqs. (7) and (8) for cubic specimens loaded in the *transversal* and *longitudinal* direction, respectively, Eqs. (9) and (10) for prisms considering strains measured from the displacement of the testing machine and displacement sensors, respectively, and Eqs. (11) and (12) for cylinders considering strains measured from the displacement of the testing machine and displacement sensors, respectively.

$$\bar{\sigma}_c(\bar{\varepsilon}_c) = \begin{cases} -1.046\bar{\varepsilon}_c{}^3 + 1.078\bar{\varepsilon}_c{}^2 + 0.968\bar{\varepsilon}_c & for \quad 0 \leq \bar{\varepsilon}_c \leq 1 \\ 0.0446\bar{\varepsilon}_c^3 - 0.1014\bar{\varepsilon}_c^2 - 0.2161\bar{\varepsilon}_c + 1.0008 & for \quad 1 < \bar{\varepsilon}_c \end{cases} \tag{7}$$

$$\bar{\sigma}_c(\bar{\varepsilon}_c) = \begin{cases} -0.562\bar{\varepsilon}_c{}^3 + 0.125\bar{\varepsilon}_c{}^2 + 1.436\bar{\varepsilon}_c & for \quad 0 \leq \bar{\varepsilon}_c \leq 1 \\ 1.1582\bar{\varepsilon}_c^3 - 0.9547\bar{\varepsilon}_c^2 - 0.0976\bar{\varepsilon}_c + 1.0000 & for \quad 1 < \bar{\varepsilon}_c \end{cases} \tag{8}$$

$$\bar{\sigma}_c(\bar{\varepsilon}_c) = \begin{cases} -1.541\bar{\varepsilon}_c{}^3 + 2.082\bar{\varepsilon}_c{}^2 + 0.458\bar{\varepsilon}_c & for \quad 0 \leq \bar{\varepsilon}_c \leq 1 \\ -0.0244\bar{\varepsilon}_c^3 - 0.2029\bar{\varepsilon}_c^2 - 0.6119\bar{\varepsilon}_c + 1.0000 & for \quad 1 < \bar{\varepsilon}_c \end{cases} \tag{9}$$

$$\bar{\sigma}_c(\bar{\varepsilon}_c) = \begin{cases} 1.000\bar{\varepsilon}_c{}^3 - 2.999\bar{\varepsilon}_c{}^2 + 2.999\bar{\varepsilon}_c & for \quad 0 \leq \bar{\varepsilon}_c \leq 1 \\ 2.6110e-4\bar{\varepsilon}_c^3 + 0.0020\bar{\varepsilon}_c^2 - 0.1080\bar{\varepsilon}_c + 1.0000 & for \quad 1 < \bar{\varepsilon}_c \end{cases} \tag{10}$$

$$\bar{\sigma}_c(\bar{\varepsilon}_c) = \begin{cases} -1.388\bar{\varepsilon}_c{}^3 + 1.777\bar{\varepsilon}_c{}^2 + 0.611\bar{\varepsilon}_c & for \quad 0 \leq \bar{\varepsilon}_c \leq 1 \\ 0.1705\bar{\varepsilon}_c^3 - 0.3153\bar{\varepsilon}_c^2 - 0.3201\bar{\varepsilon}_c + 1.0000 & for \quad 1 < \bar{\varepsilon}_c \end{cases} \tag{11}$$

$$\bar{\sigma}_c(\bar{\varepsilon}_c) = \begin{cases} 1.218\bar{\varepsilon}_c{}^3 - 3.327\bar{\varepsilon}_c{}^2 + 3.109\bar{\varepsilon}_c & for \quad 0 \leq \bar{\varepsilon}_c \leq 1 \\ -0.4475\bar{\varepsilon}_c^3 + 0.2899\bar{\varepsilon}_c^2 - 0.0769\bar{\varepsilon}_c + 1.0000 & for \quad 1 < \bar{\varepsilon}_c \end{cases} \tag{12}$$

The normalized curves are shown in Fig. 11, along with the previously normalized curves proposed by Illampas et al. [12] and by Adorni et al. [25]. In [12], the curves were obtained from compression tests on cylindrical specimens with aspect ratio value of 1. The curves obtained in this paper for the cubic specimens in the longitudinal direction, which also have a unity aspect ratio, are in very good agreement with the curves proposed in [12] for strains smaller than the peak strain. In addition, the strains in [12] were also measured by the displacement of the testing machine. However, there is a poor agreement for the post-peak part of the curve.

The results for prisms and cylinders clearly illustrate the influence of the method for measuring strains. However, cylinders and prisms provide very similar curves for both types of measuring techniques, even though the loading direction is different and there are other factors that can affect the different behavior of the cylinders (remarked in

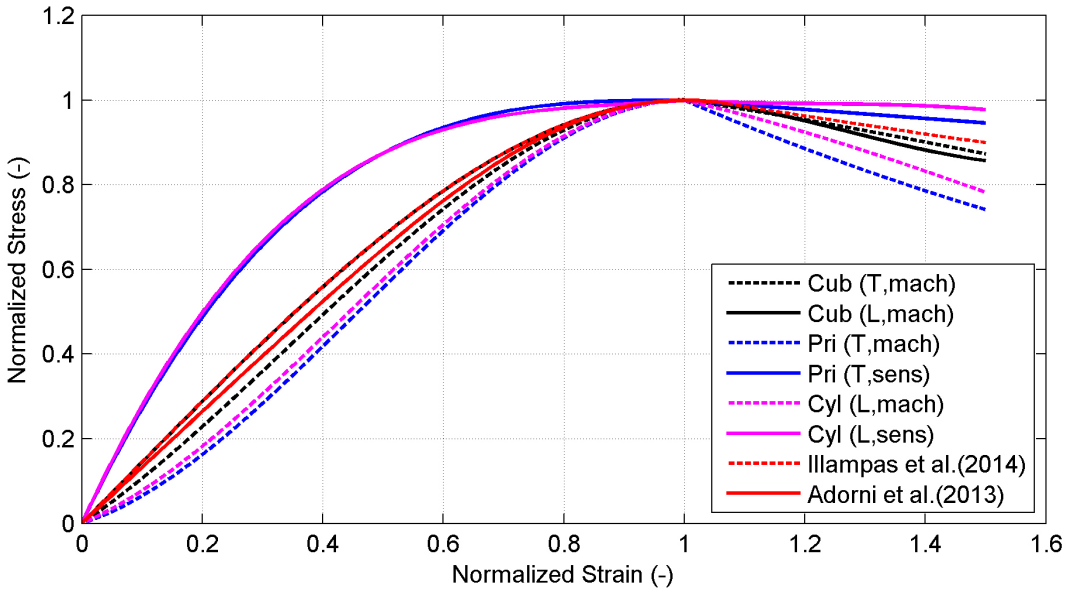

Figure 11: Normalized stress-strain relationships for each type of specimen loaded in the longitudinal (L) or transversal (T) directions and from global strain measurements from the testing machine (*mach*) or displacement sensors (sens).

section 3.1). As for the prisms and cylinders, very similar curves are obtained for the cubes loaded in the *longitudinal* and *transversal* directions. Thus, the anisotropy of the material has little effect on the normalized curves.

The curve from [25] is in between the curves for the cubes and for the cylinders and prisms obtained from displacement readings of the testing machine. The samples tested in [25] were prismatic with an aspect ratio between 1.5 and 1.8 and they were obtained by cutting samples from an archaeological site. The scattering of the specimens geometry and the results presented in [25] is very high, so they should be considered cautiously. In addition, no results are provided in [25] for strains higher than the peak strain.. Despite of this fact, they are consistent with the presented results.

Results from Fig. 11 are very promising since very similar normalized curves are obtained for different types of specimens, with different size and shape, different loading directions, and even different materials. However, the agreement between the different curves is more significant for the ascending branch of the curve than for the post-peak part. The scattering of the results increases after the compressive strength is reached. The only factors that are affecting the curves in Fig. 11 are the aspect ratio and the method for measuring strains. Therefore, by measuring just the compressive strength and the peak strains (which are easier to measure than the whole stress-strain curve), one could obtain an accurate approach of the whole stress-strain curve from the normalized curves.

4. Conclusions

This paper has analyzed the experimental compressive behavior of unfired earthen bricks made from local materials from the Guadalquivir river bank in Sevilla (Spain). Tests on whole bricks and cubic, prismatic and cylindrical specimens were carried out in the laboratories of School of Engineering of the University of Seville (Spain). Full stress-strain curves have been obtained and analyzed for all specimens. Third order polynomial curve fitting equations have been obtained for each type of test. Values of compressive strength and Young modulus have been obtained and analyzed.

Strains have been measured from the displacement of the actuator of the testing machine and from displacement sensors. The paper shows how readings from the testing machine overestimates the computed strains and lead to erroneous estimations of stress-strain curves and Young modulus.

The anisotropic behavior of the material has been identified from the different behavior observed when the load is applied in the vertical (*longitudinal*) or horizontal (*transversal*) direction during the molding process. The anisotropy affects the rigidity of the material and the compressive strength. Higher strength and lower stiffness has been obtained for specimens loaded in the *longitudinal* direction. This anisotropic behavior can be induced by the orientation of the clay platelets and the straw fibers.

The effect of the aspect ratio of the specimens on the compressive strength have been also analyzed. The obtained results show that existing correction factors for other materials may lead to erroneous estimations of the Unconfined Compressive Strength. The confinement effect might have a different influence on earthen materials because of its lower stiffness and ratio between tensile and compressive strength. Thus, existing correction factors for other materials should not be considered valid for earthen materials until a more extensive research on this issue is carried out.

The Young modulus of the material has been analyzed by obtaining values of the secant modulus at $1/3$ and $2/3$ of the compressive strength and the chord modulus between those two points. The paper has shown that previously proposed empirical correlations between Young modulus and compressive strength should not be considered as reliable since they are based on invalid strain measurements obtained from the displacement of the actuator of the testing machine. Moreover, it is highlighted the importance of specifying in any research work which estimate of Young modulus is used since very different values can be obtained for secant or tangent modulus at different points. This paper proposes the use of the tangent modulus between $1/3$ and $2/3$ of the compressive strength since it gives a good approach of the stress-strain relationship in this range.

Finally, the paper has obtained normalized stress-strain curves for each specimen. Good agreement has been obtained between different types of specimens and with results from other authors. This is a promising result that can help the standardization of methodologies for the characterization of earthen construction materials and also to develop standard constitutive models. Normalized stress-strain curves could be used to estimate the whole stress-strain curve by just determining the compressive strength and peak strain of the material.

The paper has obtained relevant conclusions for the development of methodologies for the characterization of the

compressive behavior of earthen bricks. However, it also definitely shows that further research is needed on this topic. The authors are now developing a new experimental campaign for addressing some of the open issues highlighted in this paper. This campaign also includes the experimental characterization of the mechanical behavior of adobe masonry walls in order to analyze the relationship between the compressive behavior of the bricks and the masonry.

Acknowledgments

This work was supported by the Consejería de Economía, Innovación, Ciencia y Empleo of Andalucía (Spain) under project P12-TEP-2546 and the Spanish Ministry of Economy and Competitiveness (Ministerio de Economía y Competitividad, Secretaría de Estado de Investigación, Desarrollo e Innovación) through research projects BIA2016-7531-R and BIA2016-75042-C2-1-R. The financial support is gratefully acknowledged.

References

References

[1] H. Houben, H. Guillaud, CRAterre., Intermediate Technology Publications., Earth construction : a comprehensive guide, Intermediate Technology Publications, 1994.

[2] M. Blondet, J. Vargas, N. Tarque, C. Iwaki, Seismic resistant earthen Construction: The contemporary experience at the Pontificia Universidad Católica del Perú, Informes de la Construccion 63 (523) (2011) 41–50.

[3] A.-l. Che, Z.-j. Wu, J.-j. Sun, J.-h. Qi, Seismic damage characteristics of rural adobe-wood building in Gansu province induced by the Wenchuan great earthquake, Proceedings of the International Symposium on Geoenvironmental Engineering in Hangzhou, China, September 8-10, 2009 (2009) 865–871.

[4] R. Aguilar, R. Marques, K. Sovero, C. Martel, F. Trujillano, R. Boroschek, Investigations on the structural behaviour of archaeological heritage in Peru: From survey to seismic assessment, Engineering Structures 95 (2015) 94–111. doi:10.1016/j.engstruct.2015.03.058.

[5] M. Solís, D. Torrealva, P. Santillán, G. Montoya, Análisis del comportamiento a flexión de muros de adobe reforzados con geomallas, Informes de la Construcción 67 (539) (2015) 092.

[6] H. Varum, A. Costa, J. Fonseca, A. Furtado, Behaviour Characterization and Rehabilitation of Adobe Construction, Procedia Engineering 114 (2015) 714–721. doi:10.1016/j.proeng.2015.08.015.

[7] SENCICO, Reglamento Nacional de Edificaciones. Norma Técnica de Edificación NTE 0.80 Diseño y construcción con tierra reforzada, Servicio Nacional de Capacitación para la Industrial de la Construcción, Lima, Peru, 2017.

[8] NZS, Engineering design of earth buildings. NZS 4297, Standards New Zealand, Wellington, New Zealand, 1998.

[9] J. Cid, F. R. Mazarrón, I. Cañas, Las normativas de construcción con tierra en el mundo, Informes de la Construcción (523) (2011) 159–169. doi:10.3989/ic.10.011.

[10] A. Caporale, F. Parisi, D. Asprone, R. Luciano, A. Prota, Comparative micromechanical assessment of adobe and clay brick masonry assemblages based on experimental data sets, Composite Structures 120 (2015) 208–220. doi:10.1016/j.compstruct.2014.09.046.

[11] D. Silveira, H. Varum, A. Costa, J. Carvalho, Mechanical Properties and Behavior of Traditional Adobe Wall Panels of the Aveiro District, Journal of Materials in Civil Engineering 27 (9) (2015) 04014253. doi:10.1061/(ASCE)MT.1943-5533.0001194.
URL http://ascelibrary.org/doi/10.1061/{%}28ASCE{%}29MT.1943-5533.0001194

[12] R. Illampas, I. Ioannou, D. C. Charmpis, Adobe bricks under compression: Experimental investigation and derivation of stress-strain equation, Construction and Building Materials 53 (2014) 83–90. doi:http://dx.doi.org/10.1016/j.conbuildmat.2013.11.103.

[13] E. Quagliarini, S. Lenci, The influence of natural stabilizers and natural fibres on the mechanical properties of ancient Roman adobe bricks, Journal of Cultural Heritage 11 (3) (2010) 309–314. doi:10.1016/j.culher.2009.11.012.
URL http://dx.doi.org/10.1016/j.culher.2009.11.012

[14] Q. E. Piattoni Q Lenci S, Experimental analysis and modelling of the mechanical behaviour of earthen bricks, Construction and Building Materials 25: 2067–7 (4) (2011) 2067–2075. doi:DOI:10.1016/j.conbuildmat.2010.11.039.

[15] Q.-B. Bui, J.-C. Morel, S. Hans, P. Walker, Effect of moisture content on the mechanical characteristics of rammed earth, Construction and Building Materials 54 (2014) 163–169. doi:http://dx.doi.org/10.1016/j.conbuildmat.2013.12.067.

[16] A. Laborel-Préneron, J.-E. Aubert, C. Magniont, P. Maillard, C. Poirier, Effect of Plant Aggregates on Mechanical Properties of Earth Bricks, Journal of Materials in Civil Engineering 29 (12) (2017) 04017244. doi:10.1061/(ASCE)MT.1943-5533.0002096.
URL http://ascelibrary.org/doi/10.1061/{%}28ASCE{%}29MT.1943-5533.0002096

[17] B. V. Venkatarama Reddy, V. Suresh, K. S. Nanjunda Rao, Characteristic Compressive Strength of Cement-Stabilized Rammed Earth, Journal of Materials in Civil Engineering 29 (2) (2017) 04016203. doi:10.1061/(ASCE)MT.1943-5533.0001692.
URL http://ascelibrary.org/doi/10.1061/{%}28ASCE{%}29MT.1943-5533.0001692

[18] J. E. Aubert, A. Fabbri, J. C. Morel, P. Maillard, An earth block with a compressive strength higher than 45 MPa!, Construction and Building Materials 47 (2013) 366–369. doi:10.1016/j.conbuildmat.2013.05.068.

[19] J. E. Aubert, P. Maillard, J. C. Morel, M. Al Rafii, Towards a simple compressive strength test for earth bricks?, Materials and Structures (5) (2016) 1641–1654. doi:10.13140/RG.2.1.4641.4242.

[20] D. Silveira, H. Varum, A. Costa, Influence of the testing procedures in the mechanical characterization of adobe bricks, Construction and Building Materials 40 (2013) 719–728. doi:10.1016/j.conbuildmat.2012.11.058.

[21] J. C. Morel, A. Pkla, P. Walker, Compressive strength testing of compressed earth blocks, Construction and Building Materials 21 (2) (2007) 303–309. doi:DOI:10.1016/j.conbuildmat.2005.08.021".

[22] L. Miccoli, U. Müller, P. Fontana, Mechanical behaviour of earthen materials: A comparison between earth block masonry, rammed earth and cob, Construction and Building Materials 61 (0) (2014) 327–339. doi:http://dx.doi.org/10.1016/j.conbuildmat.2014.03.009.

[23] F. Parisi, D. Asprone, L. Fenu, A. Prota, Experimental characterization of Italian composite adobe bricks reinforced with straw fibers, Composite Structures 122 (2015) 300–307. doi:http://dx.doi.org/10.1016/j.compstruct.2014.11.060.

[24] D. Silveira, H. Varum, A. Costa, T. Martins, H. Pereira, J. Almeida, Mechanical properties of adobe bricks in ancient constructions, Construction and Building Materials 28 (1) (2012) 36–44. doi:http://dx.doi.org/10.1016/j.conbuildmat.2011.08.046.

[25] E. Adorni, E. Coïsson, D. Ferretti, In situ characterization of archaeological adobe bricks, Special Section on Recycling Wastes for Use as Construction Materials 40 (2013) 1–9. doi:http://dx.doi.org/10.1016/j.conbuildmat.2012.11.004.

[26] R. Aguilar, M. Montesinos, S. Uceda, Mechanical characterization of the structural components of Pre-Columbian earthen monuments: Analysis of bricks and mortar from Huaca de la Luna in Perú, Case Studies in Construction Materials 6 (2017) 16–28. doi:10.1016/j.cscm.2016.11.003.

[27] CNS, EN 772-1. Methods of test for masonry units (Part 1: Determination of compressive strength), European Committee for Standardization, Brussels, Belgium, 2011.

[28] A. Eslami, H. R. Ronagh, S. S. Mahini, R. Morshed, Experimental investigation and nonlinear FE analysis of historical masonry buildings - A case study, Construction and Building Materials 35 (2012) 251–260. doi:10.1016/j.conbuildmat.2012.04.002.

[29] P. Maillard, J. E. Aubert, Effects of the anisotropy of extruded earth bricks on their hygrothermal properties, Construction and Building Materials 63 (2014) 56–61. doi:10.1016/j.conbuildmat.2014.04.001.

[30] J. Bourret, N. Tessier-Doyen, R. Guinebretiere, E. Joussein, D. S. Smith, Anisotropy of thermal conductivity and elastic properties of extruded clay-based materials: Evolution with thermal treatment, Applied Clay Science 116-117 (Supplement C) (2015) 150–157. doi:https://doi.org/10.1016/j.clay.2015.08.006.
URL http://www.sciencedirect.com/science/article/pii/S0169131715300739

[31] W. Krefeld, Effect of shape of specimen on the apparent compressive strength of brick masonry, Proceedings of the American Society of

Materials, Philadelphia p (1938) 363–369.

[32] K. Heathcote, E. Jankulovski, Aspect ratio correction factors for soilcrete blocks, Transactions of the Institution of Engineers, Australia. Civil engineering 34 (4) (1992) 309–312.

[33] AENOR, UNE 41410: Bloques de tierra comprimada para muros y tabiques: definiciones, especificaciones y métodos de ensayo, Asociación Española de Normalización y Certificación, Madrid, Spain, 2008.

[34] AENOR, UNE 22-950-90 Parte 3. Propiedades mecánicas de las rocas. Ensayos para la determinación de la resistencia. Parte 3: Determinación del módulo de elasticidad (Young), Asociación Española de Normalización y Certificación, Madrid, Spain, 1993.

[35] ASTM, Standard Test Method for Young's Modulus, Tangent Modulus, and Chord Modulus. E111-04, ASTM International, West Conshohocken, Penn., United States, 2004 (Reapproved 2010).